Inferring Asymmetric Relations between Interacting Neuronal Oscillators

Laura CIMPONERIU,[1] Michael G. ROSENBLUM,[2] Thomas FIESELER,[3] Jürgen DAMMERS,[3] Michael SCHIEK,[4] Milan MAJTANIK,[3] Patricia MOROSAN,[3] Anastasios BEZERIANOS[1] and Peter A. TASS[3,5]

[1]*Department of Medical Physics, University of Patras, 26 500 Rion Patras, Greece*
[2]*Department of Physics, University of Potsdam, D-14415 Potsdam, Germany*
[3]*Institute of Medicine, Research Centre Jülich, D-52425 Jülich, Germany*
[4]*Central Electronics Laboratory, Research Centre Jülich, D-52425 Jülich, Germany*
[5]*Department of Stereotaxic and Functional Neurosurgery, University of Cologne, 50924 Cologne, Germany*

We apply a quantitative method for the identification of asymmetric relations between weakly interacting self-sustained oscillators to the study of rhythmic neural electrical activity. We begin by testing the method on biophysically motivated neural oscillator models considering first two diffusively coupled Hindmarsh-Rose oscillators, and then two ensembles of globally coupled neurons interacting through their mean fields. Next, we consider the more complex case of interactions among several oscillatory units. The method is further applied to the analysis of the control of externally vs internally paced movements in humans. A pilot study in one healthy subject reveals that asymmetry of interactions between different brain areas may strongly change with the transition from external to internal pacing, while the degree of synchronization hardly changes. Furthermore, our preliminary results highlight the important role of the secondary auditory cortex in internal rhythm generation.

§1. Introduction

Nonlinear dynamics and coupled oscillators theory have provided fundamental ideas and tools for the analysis of complex experimental data.[1)–3)] An important application of these tools is the study of brain activity at different levels of neuronal organization, from the cellular level up to large scale neuronal networks.[4)–10)] Numerous theoretical studies have been devoted to understanding how inter-cellular coupling mechanisms in conjunction with intrinsic properties of the neurons account for experimentally observed coherent, rhythmical behavior in neuronal populations.[11),12)] This knowledge could further illuminate on the functional role of interaction between different populations in brain information processing, both in normal and pathological conditions. The ultimate goal of the research in this field is to translate theoretical knowledge into novel noninvasive diagnostic tools (e.g., synchronization tomography[13)]) and therapeutic techniques (e.g., demand-controlled desynchronizing deep brain stimulation based on stochastic phase resetting[14)–16)]).

Rhythmical phenomena in the electrical activity of the brain can be often understood within the framework of the coupled oscillators theory. This formalism has provided explanation for a number of observed synchronization phenomena and coherent behavior in neuronal ensembles. In addition, techniques derived from synchronization theory have found useful applications in the analysis of brain electrical

activity.[5),17),18)]

Non-invasive brain recordings are typically multichannel measurements of electric (electroenchephalogram, EEG) or magnetic brain activity (magnetoenchephalogram, MEG) which reveal the coexistence of broad-band activity and rhythms of different frequencies. In the multivariate analysis of these signals we can outline two important tasks. The first task is to reveal and quantify interaction between certain sources of oscillatory activity.[3),5),17),19)–21)] Once the presence of interaction is established or physiologically motivated, the second task is to identify the asymmetry, or the direction of coupling between these sources, i.e., to find out which of the interacting oscillators predominantly effects its counterpart.

An approach that enables the identification of the asymmetry of weak interaction of self-sustained oscillators has been developed quite recently.[22),23)] In the present study, we evaluate the performance of the proposed method using biophysically motivated models. Further, we apply this method to the analysis of asymmetry of the interaction of sources of rhythmic neural activity engaged in the control of externally vs internally paced movements. MEG and EMG (electromyographic) measurements have been performed in a healthy subject during a paced finger tapping (PFT) experiment.[24)] The subject was first asked to tap with his index finger in synchrony with a periodic train of tones (external pacing). After discontinuing the tones, the subject continued the periodic finger tapping, guided by internal timing mechanism. The brain areas active during PFT were consistently localized with functional magnetic resonance imaging (fMRI), which detects neuronal activity indirectly by measuring an increase of the blood oxygenation level,[25)] and with synchronization tomography,[13)] i.e., a phase synchronization analysis[5)] applied to the cerebral current source density, reconstructed with magnetic field tomography.[26)] Unlike fMRI, the synchronization tomography enables to study interactions between different brain areas, as well as between brain areas and muscular activity. In this way four relevant neural sources have been selected for further analysis.

The paper is organized as follows. In §2 we briefly describe the algorithms. Section 3 is devoted to tests of the algorithms on the models of neuronal oscillators. We start here with the case of two interacting neuronal oscillators. Then we propose a model of two interacting sources of neural activity. For this purpose we consider each source as a population of globally coupled neurons, generating a macroscopic mean field; next we assume that the populations interact through their mean fields. Finally, we treat the case of several interacting units. In §4 we present the experiment, the algorithmic steps of data processing and the results of asymmetry analysis. In §5 we discuss our results.

§2. Quantification of directionality from bivariate data

Traditional techniques of data analysis do not provide information on directional relations between systems. This problem can be approached from the viewpoint of information theory; direction of interaction can then be described in terms of mutual predictability or information transfer.[27)–29)] Another approach is based on the notion of dynamical interdependence,[4)] i.e., on existence of a functional relationship between

the points in the (reconstructed) phase spaces of two systems; this relationship can be asymmetrical. The latter approach is tightly related to the notion of generalized synchronization and can be also described in terms of mutual predictability.[18)]

Here we briefly describe our previously developed approach[22),23)] and then apply it to the analysis of neuronal electrical activity. This approach is based on the assumption that the systems under investigation can be regarded as weakly coupled self-sustained oscillators. Such an assumption makes this approach more restrictive compared to the approach based on the information theory. However, as models of coupled oscillators describe a variety of natural phenomena, our technique can be used in many practical situations offering some advantages over other methods, like simplicity of implementation and interpretation, ability to work with rather short and noisy data, small number of parameters. The starting point is one of the main ideas of the coupled oscillators theory: Weak coupling influences the phase dynamics, without altering each oscillator's intrinsic limit cycle. Thus, the interaction, though weak, leads to qualitative change in the collective dynamics. This property enables the reduced description of two weakly interacting oscillators by the phase model:

$$\dot{\phi}_{1,2} = \omega_{1,2} + \varepsilon_{1,2} f_{1,2}(\phi_{1,2}, \phi_{2,1}) + \xi_{1,2}(t) \ , \tag{2·1}$$

where $\phi_{1,2}(t)$ denote the continuous phase variables (defined on the whole real line, not on the $[0, 2\pi)$ circle).[30)] The coupling is described through the 2π-periodic functions $f_{1,2}$ which also incorporate the properties of individual oscillators. The strength of coupling is given by the parameters $\varepsilon_{1,2} \ll \omega_{1,2}$. Recently it has been shown that complex (aperiodic) oscillators admit a similar description if a suitable phase variable can be defined.[31)] The terms $\xi_{1,2}$ in (2·1) account for amplitude fluctuations in aperiodic (chaotic) oscillators and/or random perturbations which are always present in the real-world systems.

We emphasize that there is no unique way to quantify the directionality of coupling, even if Eq. (2·1) is known. Clearly, if one of the parameters $\varepsilon_{1,2}$ is zero, then the coupling is unidirectional. However, if $\varepsilon_{1,2} \neq 0$, quantification of asymmetry becomes ambiguous. We call interaction symmetric if the coupling terms are identical (i.e. $\varepsilon_1 f_1(\cdot) = \varepsilon_2 f_2(\cdot)$), what however does not take into account the difference of natural frequencies $\omega_{1,2}$. We quantify the influence of system 2 on system 1 by the coefficient $c_1^2 = \langle(\partial\dot{\phi}_1/\partial\phi_2)^2\rangle = \varepsilon_1^2\langle(\partial f_1/\partial\phi_2)^2\rangle$, where $\langle(\cdot)\rangle = \int\int_0^{2\pi}(\cdot)d\phi_1\, d\phi_2$ denotes averaging over $\phi_{1,2}$. c_1 is an integrative measure of how strongly oscillator 1 is driven and how sensitive it is to the driving. Computing in the same way c_2, we quantify asymmetry in interaction by one number

$$d^{(1,2)} = \frac{c_2 - c_1}{c_1 + c_2} \ , \tag{2·2}$$

that we call *directionality index*. It varies from 1 in the case of unidirectional coupling $(1 \to 2)$ to -1 in the opposite case $(2 \to 1)$, while intermediate values correspond to a bi-directional coupling configuration. If two oscillators are structurally identical and differ only by natural frequencies then $f_1(\cdot) = f_2(\cdot)$ and $d^{(1,2)} = (\varepsilon_2 - \varepsilon_1)/(\varepsilon_1 + \varepsilon_2)$.

Practically, we proceed as follows. Taking time series of phases $\phi_{1,2}$ that can be

estimated from data (see below) we construct new time series

$$\Delta_{1,2}(k) = \phi_{1,2}(t_k + \tau) - \phi_{1,2}(t_k) \ , \tag{2·3}$$

where τ is the only parameter. Phase increments $\Delta_{1,2}$ can be considered as generated by an unknown two-dimensional noisy map, analogue of continuous time Eq. (2·1):

$$\Delta_{1,2}(k) = \mathcal{F}_{1,2}\left(\phi_{1,2}(t_k), \phi_{2,1}(t_k)\right) + \eta_{1,2}(t_k) \ . \tag{2·4}$$

The functions $\mathcal{F}_{1,2}$ can be estimated from data. Indeed, as they are periodic with respect to phases, they can be approximated by a finite double Fourier series. Coefficients of this series can be obtained by fitting the dependencies of $\Delta_{1,2}$ on $\phi_{1,2}$ in the least mean square sense. Notice that fitting has also a noise reduction effect.[32] Denoting the approximates of $\mathcal{F}_{1,2}$ by $F_{1,2}$, computing analytically the derivatives $\partial F_{1,2}/\partial\phi_{2,1}$, and averaging, we estimate the coefficients

$$c_{1,2}^2 = \left\langle \left(\frac{\partial F_{1,2}}{\partial \phi_{2,1}} \right)^2 \right\rangle \tag{2·5}$$

and directionality index according to Eq. (2·2). Concerning the choice of τ, we mention that in the weak coupling ($\varepsilon_{1,2} \ll \omega_{1,2}$) regime, the deviation of the phase growth from ωt becomes significant only on a time scale comparable to the oscillatory period. We take τ equal to the mean period of the fastest oscillator, following previous insight[23] into the parameter selection problem.

We emphasize that the algorithm fails if the oscillators are phase locked, which mathematically corresponds to the appearance of a functional dependence between the two phase variables. Alternative solutions of the directionality estimates have been discussed and experimentally verified in Refs. 23), 33).

The described approach requires the knowledge of the phases of the interacting systems. Therefore, the first step in the analysis of experimental data is an estimation of the instantaneous phases from the signals. This can be done by means of the Hilbert transform (see discussion and technical details in Ref. 3)) or complex continuous wavelet transform;[6] these methods appear to be nearly equivalent if applied in synchronization analysis.[34] Alternatively, the phase can be determined via marker events in time series, in analogy to the Poincaré section technique. Indeed, if a time series contains some easily detectable marker event per each oscillation period, e.g. a spike, then the period can be associated with the inter-spike interval. Correspondingly, we can assign 2π phase increment to each inter-spike interval and obtain the instantaneous phase by linear interpolation between the spikes:[3]

$$\phi(t) = 2\pi \cdot \frac{t - t_k}{t_{k+1} - t_k} + 2\pi \cdot k \ , \tag{2·6}$$

where t_k are the instants of spike occurrence in the signal. Below we discuss the choice of a suitable technique.

§3. Testing the algorithm with models of neuronal oscillations

The application of the directionality identification algorithm to electrophysiological data, and especially brain activity, suggests to test this algorithm on biophysically motivated neuron models.

3.1. *Two coupled neuronal oscillators*

We begin by considering the Hindmarsh-Rose (HR)[35] neuron model which, with minimal complexity (i.e., three variables only) replicates the main dynamical regimes of regular spiking and chaotic spiking-bursting activity observed in living neurons.

Two electrically coupled HR neurons are described by the following set of coupled ordinary differential equations:

$$\begin{aligned} \dot{x}_{1,2} &= y_{1,2} - x_{1,2}^3 + 3x_{1,2}^2 - z_{1,2} + I_{1,2} + \varepsilon_{1,2}(x_{2,1} - x_{1,2}) \ , \\ \dot{y}_{1,2} &= 1 - 5x_{1,2}^2 - y_{1,2} \ , \\ \dot{z}_{1,2} &= 0.006 \cdot (4(x_{1,2} + 1.6) - z_{1,2}) \ . \end{aligned} \tag{3·1}$$

The x variable represents the membrane potential, y is a recovery variable and z represents the internal mechanism which regulates the patterns of discharges. The parameters $I_{1,2}$ denote the external current injected to each neuron; the spiking frequency is approximately proportional to I. In our simulation we set $I_1 = 5$, $I_2 = 5.2$; for these parameters an individual cell exhibits periodic spiking. Parameters $\varepsilon_{1,2}$ denote the strength of the synaptic coupling. For the tests, we fixed $\varepsilon_1 = 0.05$, and varied ε_2 in the interval $[0, 0.5]$.

With increase of the coupling strength (parameter ε_2), the two oscillators exhibit different regimes of spiking. So, periodic spiking (like in uncoupled neurons) is preserved at very weak coupling and re-established in the synchronous regime, whereas a bursting behavior (short trains of spikes intercalated by quiescent intervals) is observed for intermediate coupling strength. Figure 1 shows typical spiking patterns encountered within the explored range of the coupling strength. The results of the directionality analysis are shown in Fig. 2(a). For each coupling configuration explored, the index $d^{(1,2)}$ was computed from the instantaneous phases of signals $x_{1,2}$; the length of data corresponds to ≈ 200 consecutive spikes. Instantaneous phases have been computed according to Eq. (2·6).

Note that transition to synchronization is not monotonic here. This can be observed in Fig. 2(b), where we plot synchronization index $\rho^2 = \langle \cos(\phi_1(t) - \phi_2(t) \rangle^2 + \langle \sin(\phi_1(t) - \phi_2(t)) \rangle^2$, that is the intensity of the first Fourier mode of the phase difference distribution; brackets $\langle \ \rangle$ denote time averaging. $\rho = 1$ means perfect locking, whereas $\rho = 0$ corresponds to the absence of interaction. The unusual behavior of the synchronization index is caused by non-monotonic changes in the firing period that occur at small coupling strength between the two oscillators. However, the directionality index correctly identifies the asymmetry in interaction, independently of the dynamical regime (regular spiking or spiking-bursting).

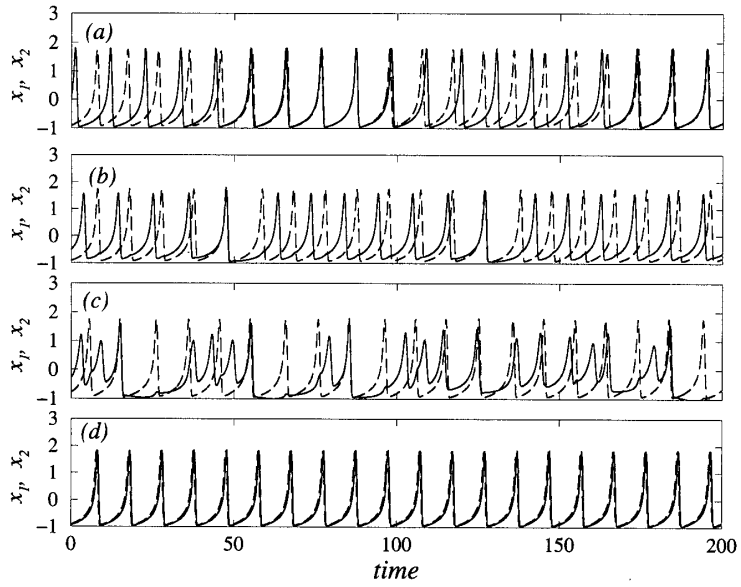

Fig. 1. Time series of x variables from coupled HR oscillators (Eqs. (3·1)) with $\varepsilon_1 = 0.05$ kept constant and ε_2 varied: (a) $\varepsilon_2 = 0$, (b) $\varepsilon_2 = 0.1$, (c) $\varepsilon_2 = 0.3$, and (d) $\varepsilon_2 = 0.4$.

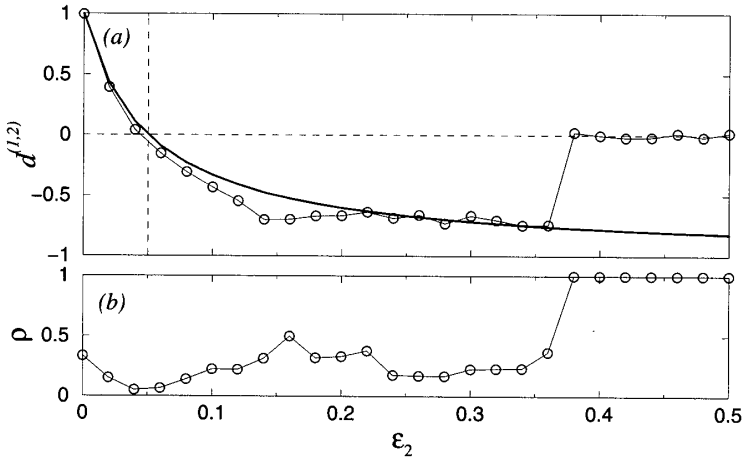

Fig. 2. Dependence of (a) the directionality index $d^{(1,2)}$ and (b) the synchronization index ρ on ε_2 for two coupled HR oscillators with fixed $\varepsilon_1 = 0.05$. Solid line in (a) shows the theoretical curve for $d^{(1,2)}$ according to $(\varepsilon_2 - \varepsilon_1)/(\varepsilon_1 + \varepsilon_2)$. Note that estimation of $d^{(1,2)}$ is effective unless the two systems synchronize.

3.2. *Two coupled ensembles of neuronal oscillators*

Modeling sources of rhythmic activity that contribute to MEG and EEG generation implies a macroscopic level of description, i.e., consideration of the dynamics of large neuronal ensembles. It is widely believed that the onset of rhythmical activity in a population of neurons can be regarded as the Kuramoto transition[30),36)] in an ensemble of globally (each-to-each) coupled oscillators.[37)] Correspondingly, interaction of two (or several) sources of brain activity can be modeled by two (or several) interacting ensembles.

In order to test the applicability of our approach to MEG signals, we consider two populations of N globally coupled oscillators; the populations diffusively interact

through their mean fields. We start with the simplest model of an individual neuron, the FitzHugh-Nagumo, or Bonhoeffer-van der Pol oscillator. The equations of the model are:

$$\begin{aligned} \dot{x}_i &= x_i - x_i^3/3 - y_i + I_i + \eta X + \varepsilon_1(U - X) , \\ \dot{y}_i &= 0.1 \cdot (x_i + 0.7 - 0.8 y_i) , \\ \dot{u}_i &= u_i - u_i^3/3 - v_i + J_i + \eta U + \varepsilon_2(X - U) , \\ \dot{v}_i &= 0.1 \cdot (u_i + 0.7 - 0.8 v_i) . \end{aligned} \tag{3·2}$$

Here the variables x_i, y_i and u_i, v_i, where $i = 1, \cdots, N$, describe the ith elements of the first and second population, respectively; $X = N^{-1} \sum_{i=1}^{N} x_i$ and $U = N^{-1} \sum_{i=1}^{N} u_i$ are the mean fields of the populations. Parameter η denotes the coupling within each population (for simplicity we suppose it to be the same in each population), while $\varepsilon_{1,2}$ describe the coupling between the two ensembles. Parameters I_i, J_i correspond to external currents injected into each neuron of the first and second population, respectively; they determine the spiking frequency of the individual neurons. We further assume that neurons within each population are subject to different inputs I_i and J_i, respectively. I_i, J_i are assumed to be Gaussian distributed numbers with the mean values $\bar{I} = 0.6$ and $\bar{J} = 0.7$, and standard deviation $\Delta I = \Delta J = 0.01$. For the chosen value of $\eta = 0.005$, a non-zero mean field occurs in each ensemble. As $\bar{I} \neq \bar{J}$, then in the absence of coupling between ensembles ($\varepsilon_{1,2} = 0$), the mean fields have different frequencies.

Table I. Results of the directionality estimates for the coupled populations model (3·2); $d_{\text{th}}^{(1,2)}$ is the theoretical prediction $(\varepsilon_2 - \varepsilon_1)/(\varepsilon_1 + \varepsilon_2)$.

ε_1	ε_2	$d_{th}^{(1,2)}$	$d^{1,2}$
0.001	0.001	0	0.05
0.002	0.002	0	0.07
0	0.002	1	0.99
0.001	0.002	0.33	0.38

A Kuramoto transition in a population of globally coupled oscillators appears as a Hopf bifurcation for the mean field (i.e. the order parameter). Therefore, the dynamics of two coupled populations should be similar to the dynamics of two coupled self-sustained oscillators.[38] A detailed analysis of a model of coupled populations is beyond the framework of this paper; here we just simulate the model (3·2) for $N = 500$ and for different values of $\varepsilon_{1,2}$, testing the efficiency of the asymmetry detection. For the estimation of $d^{(1,2)}$ we take the mean fields X, U as the signals and estimate the instantaneous phases by means of the Hilbert Transform. For sufficiently large coupling strength we observe synchronization between the populations; in this regime the directionality cannot be detected (see the discussion in §2). For coupling strength below synchronization threshold asymmetry is reliably detected, as exemplified by results in Table I.

For the next test, we consider two coupled ensembles of Hindmarsh-Rose neu-

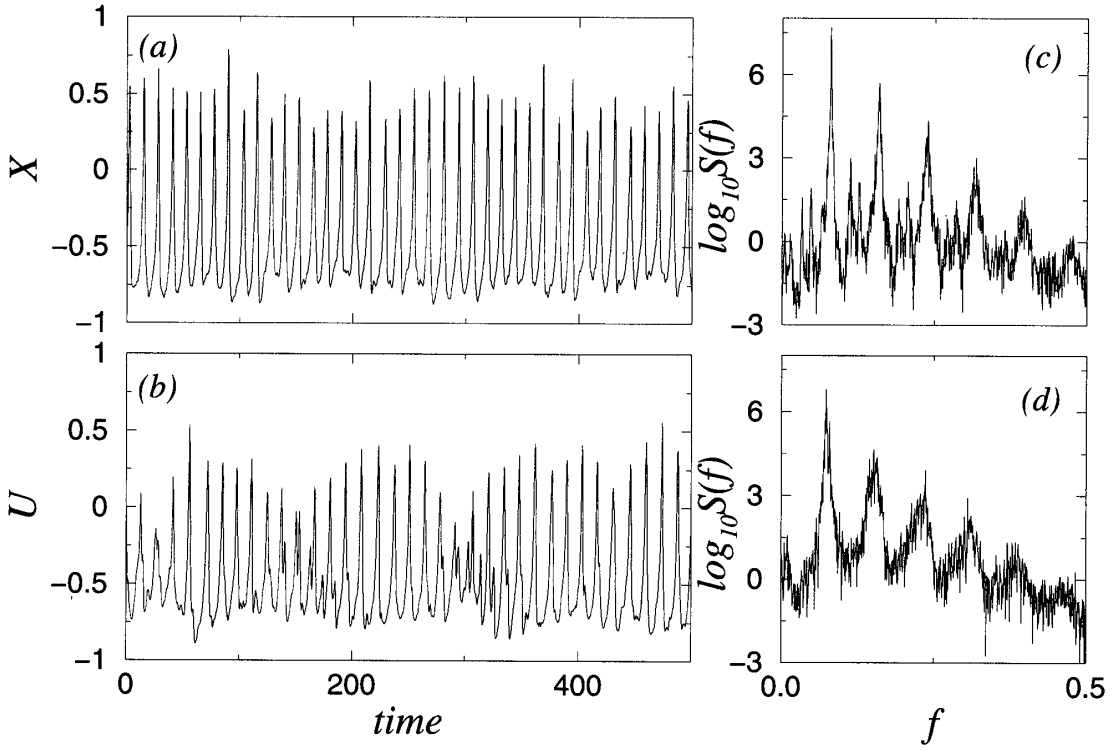

Fig. 3. Mean fields X (a) and U (b) in two interacting ensembles of HR neurons for $\varepsilon_1 = 0.05$ and $\varepsilon_2 = 0.07$ and their power spectra (c), (d).

rons:

$$\begin{aligned}
\dot{x}_i &= y_i - x_i^3 + 3x_i^2 - z_i + I_i + \eta X + \varepsilon_1(U - X) \ , \\
\dot{y}_i &= 1 - 5x_i^2 - y_i \ , \\
\dot{z}_i &= 0.006 \cdot (4(x_i + 1.6) - z_i) \ , \\
\dot{u}_i &= v_i - u_i^3 + 3u_i^2 - w_i + J_i + \eta U + \varepsilon_2(X - U) \ , \\
\dot{v}_i &= 1 - 5u_i^2 - v_i \ , \\
\dot{w}_i &= 0.006 \cdot (4(u_i + 1.6) - w_i) \ ,
\end{aligned} \tag{3·3}$$

where variables x_i, y_i, z_i and u_i, v_i, w_i describe the dynamics of the ith neuron in the first and second population, respectively, and $X = N^{-1}\sum_1^N x_i$ and $U = N^{-1}\sum_1^N u_i$ are the mean fields. Other parameters have the same meaning as in Eqs. (3·2). The values of the currents I_i and J_i are assumed to be Gaussian distributed around the mean values $\bar{I} = 5$ and $\bar{J} = 5.1$ with standard deviation $\Delta I = \Delta J = 0.05$. In this range of parameters individual neurons exhibit periodic spiking with the frequency approximately linearly increasing with the magnitude of the input current.

We performed numerical simulations of Eqs. (3·3) with $N = 1000$ oscillators in each population and the global coupling parameter $\eta = 0.5$ above the critical value for which a finite macroscopic mean field occurs in each ensemble. One inter-population coupling coefficient has been fixed, $\varepsilon_1 = 0.05$, while ε_2 was varied in the interval $[0, 0.11]$.

It is well-known that the dynamics of the mean field can be complex: examples

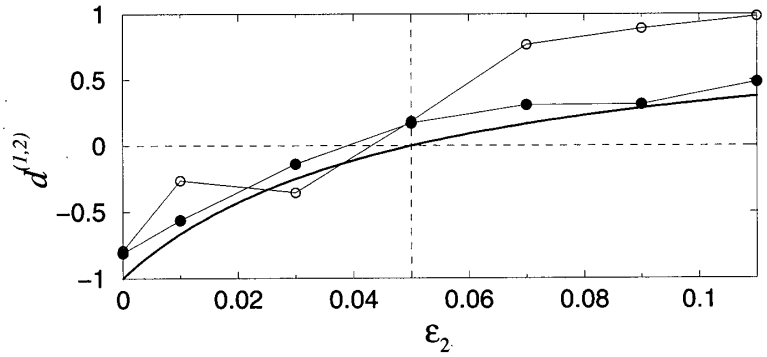

Fig. 4. Dependence of directionality index $d^{(1,2)}$ on ε_2 for two coupled ensembles of HR oscillators. Symbols ○ and • denote estimates with phases determined via Poincaré section and Hilbert transform, respectively. The bold line shows the curve $(\varepsilon_2 - \varepsilon_1)/(\varepsilon_1 + \varepsilon_2)$.

are formation of clusters,[39] dephasing and bursting[40] and collective chaos.[41),42] In our model the mean field appears to be irregular (Fig. 3). Without going into details of the collective dynamics of the HR neurons, we estimated the directionality index considering the mean fields X, U as observables. Estimation of the instantaneous phase from such complex mean field data requires a careful consideration. The mean field appears as a sequence of large and small spikes. It is not clear whether 2π phase increment should be attributed to each spike. Indeed, if phase variables have been computed via the marker events technique, the directionality estimates largely deviate from the theoretical prediction (see Fig. 4, ○ symbols). To overcome the difficulty in accurate phase estimation from original mean field data, we filtered the signals with a bandpass linear-phase FIR filter centered on the frequency of the dominant spectral component (see Figs. 3(c) and (d)). In this way, we obtained a narrow-band process with a well-defined phase. Instantaneous phases have further been estimated using the Hilbert transform of the filtered data. This approach has lead to a considerably increased accuracy of the directionality index estimates, as it can be observed in Fig. 4 (• symbols).

3.3. *From two coupled oscillators to a complex network*

Our algorithm has been designed for the case of two coupled oscillators. However, a complex natural system, like the human brain, may represent a complex network of N oscillators. Theoretically, we can write for each oscillator, similarly to Eq. (2·4),

$$\Delta_i(k) = \mathcal{F}_i\left(\phi_1(t_k), \cdots, \phi_N(t_k)\right) + \eta_i(t_k) \ ,$$

compute coefficients $c_{i,j}$ and $c_{j,i}$, and directionality indices $d^{(i,j)}$ for each pair i, j of oscillators, where $i, j = 1, \cdots, N$ and $i \neq j$. However, for large N the approach requires a multidimensional regression and becomes computationally very inefficient.

Simple tests show that a pairwise analysis provides reasonable results in case of complex networks as well. One test was performed in Ref. 23), where a ring of three unidirectionally coupled oscillators was considered. Here we analyze two

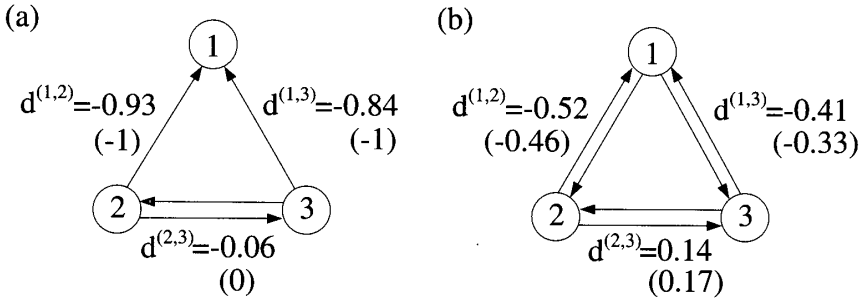

Fig. 5. Different coupling configurations of three oscillators. Parameters of coupling are given in the text. The numbers in brackets show the value $(\varepsilon_{ji} - \varepsilon_{ij})/(\varepsilon_{ij} + \varepsilon_{ji})$.

configurations (Fig. 5) in a system of three coupled Bonhoeffer-van der Pol oscillators:

$$\begin{aligned} \dot{x}_i &= x_i - x_i^3/3 - y_i + I_i + \varepsilon_{ij}(x_j - x_i) + \varepsilon_{ik}(x_k - x_i) \,, \\ \dot{y}_i &= 0.1 \cdot (x_i + 0.7 - 0.8 y_i) \,, \end{aligned} \tag{3·4}$$

where $i, j, k = 1, 2, 3$ and $i \neq j \neq k$. The natural frequency of each oscillator has been set by parameters $I_1 = 0.5$, $I_2 = 0.55$, and $I_3 = 0.6$, respectively. The first configuration (Fig. 5(a)) considers symmetric ($\varepsilon_{23} = \varepsilon_{32} = 0.0015$) and unidirectional ($\varepsilon_{12} = 0.002$, $\varepsilon_{13} = 0.001$) coupling between the elements of the network, while the second one (Fig. 5(b)) exemplify the case of asymmetric mutual interactions ($\varepsilon_{12} = 0.0011$, $\varepsilon_{21} = 0.003$, $\varepsilon_{23} = 0.002$, $\varepsilon_{32} = 0.001$, $\varepsilon_{13} = 0.001$, $\varepsilon_{31} = 0.002$). We observe that the pairwise analysis of interactions correctly identifies the specific configuration of the network. Difficulty in evaluating the accuracy of $d^{(i,j)}$ estimates is related to the inability of the pairwise analysis to resolve the contribution of the third oscillator, leaving unknown the theoretical prediction of the directionality index.

Before presenting the analysis of experimental data, we would like to underline two points that are essential for reliability and correct interpretation of the results. First, we emphasize that the algorithm requires that the phase is well-defined, i.e., one can unambiguously identify oscillation cycles in the signal. This requirement is more strict than, e.g., in case of the computation of the synchronization index. The second point concerns the interpretation of the index that generally is determined both by parameters of $\varepsilon_{1,2}$ and functions $f_{1,2}$ in the model (2·1). So, it is possible that the asymmetry in $f_{1,2}$ dominates over the asymmetry in $\varepsilon_{1,2}$. This may lead to counterintuitive results when, say, for $\varepsilon_1 > \varepsilon_2$ the index d is positive. Indeed, d quantifies the integrative effect of how strongly each of the oscillators is driven by its counterpart and of how sensitive it is to this driving. In other words, our approach quantifies the average influence of each oscillator on the phase dynamics of the other one.

§4. Brain activity during paced finger tapping

We apply the directionality analysis to the study of cerebro-muscular and cerebro-cerebral processes engaged in sensory-motor coordination during a paced finger tap-

ping experiment. Pairwise interactions between four relevant neural sources of rhythmical electrical activity are evaluated for directionality, under two different conditions of the same experiment: external and internal pacing. MEG and EMG measurements were performed in a healthy male subject. During the first minute the subject had to tap with his right index finger in synchrony with an external cue administered at 2 Hz (external pacing). During the second minute the external pacing was terminated, and the subjects had to continue the tapping with the same rate as during the first minute (internal pacing).

4.1. *Data acquisition, pre-processing, and synchronization tomography*

EMG and MEG signals were registered with a sampling rate of 1017.25 Hz. The EMG was recorded from the right flexor digitorum muscle (RF). A standard preprocessing of the raw EMG signal, i.e., a high-pass filtering (> 30 Hz) followed by rectification (where $x \to |x|$) and a band-pass filtering of the dominant frequency peak (1 Hz–3 Hz), was applied to extract the burst activity, so that the resulting signal represents the time course of the task-related muscular activity (see Ref. 13)).

In a previous study we determined the brain areas which were synchronized with the muscular activity during the paced finger tapping by means of the *synchronization tomography*,[13] i.e., a phase synchronization analysis[5] applied to the current source density obtained from the measured MEG signals with magnetic field tomography.[26] This has been done in two steps:

1. Reconstruction of the cerebral current source density: The cerebral current source density (CSD) which generates the measured magnetic field was calculated in each volume element (voxel) and for all times t with magnetic field tomography (MFT).[26] This computationally demanding single-run analysis runs on a supercomputer (Cray T3E).

2. Synchronization analysis: Phase synchronization was analyzed voxel by voxel by computing the synchronization index:[5] To detect cerebro-muscular synchronization, the degree of phase synchronization between the muscular activity (the recorded EMG signal) and CSD was determined in each of the voxels representing the brain, whereas for cerebro-cerebral synchronization the phase relation was computed between all pairs of voxels. For the phase synchronization analysis the dominant frequency components were extracted with band-pass FIR filters between 1 Hz and 3 Hz as well as between 3 Hz and 5 Hz corresponding to dominant peaks in the frequency spectrum around 2 Hz and around 4 Hz. Figures 6 and 7 show power spectra and coherence function of RF and SMC as well as SMC and LC, respectively.

Along the lines of a pilot study we here focus on the interaction of the 2 Hz activity (i.e. the CSD in the range of 1–3 Hz) of four areas which displayed strongest cerebro-muscular synchronization: left premotor cortex (PMC), left sensorimotor cortex (SMC, consisting of primary motor and primary sensory cortex), left secondary auditory cortex (SAC), and left cerebellum (LC). For the asymmetry analysis we only used the component of the CSD vector which displayed the most pronounced frequency peak around 2 Hz.

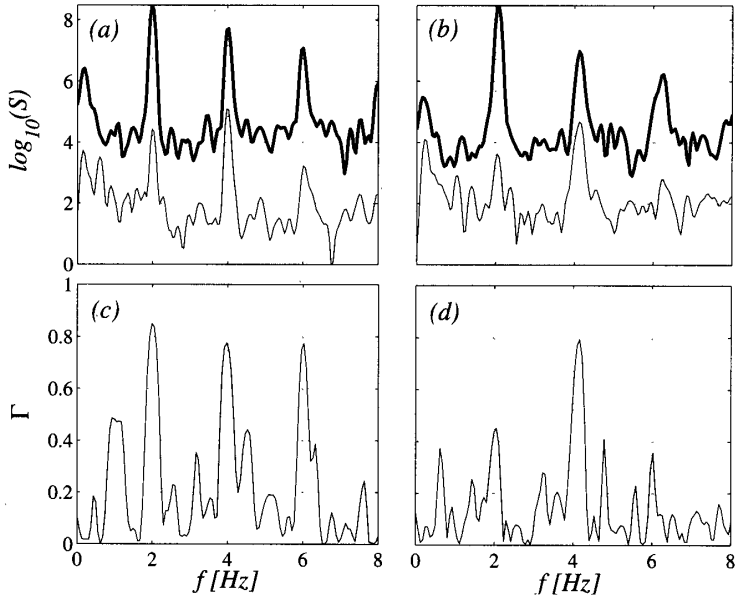

Fig. 6. Power spectra (a), (b) and coherence function (c), (d) of muscular activity (RF, bold line) and sensorimotor cortex (SMC, thin line) during external pacing (a), (c) and internal pacing (b), (d). For better visualization the spectra of two signals have been plotted with an offset.

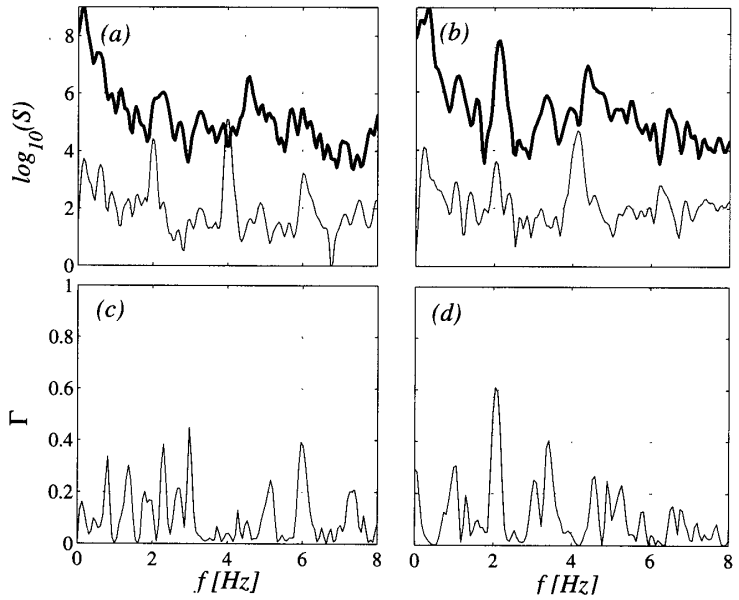

Fig. 7. Power spectra (a), (b) and coherence function (c), (d) of cerebellar activity (LC, bold line) and sensorimotor cortex (SMC, thin line) during external pacing (a), (c) and internal pacing (b), (d).

4.2. *Results*

The main results are summarized in Fig. 8, where we show the difference of the asymmetry and strength of interaction of the four areas during external and internal pacing. The four areas are associated with time estimation (LC), movement coordination (PMC, LC), and inner voice (SAC). Remarkably, in the analyzed 2 Hz-range the phase synchronization hardly differs for the two conditions (Fig. 8(b)), whereas the directionality changes strongly (Fig. 8(a)). For the interpretation of the

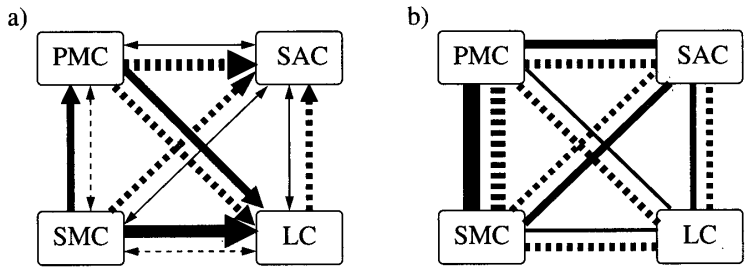

Fig. 8. Quantitative analysis of pairwise interactions of brain sources: Asymmetry analysis (a) and phase synchronization analysis (b) of the four cerebral areas. (a) Direction is indicated by the connecting arrow, where the degree of asymmetry is coded by the width of the arrow. A symmetric relationship is indicated by a bidirectional arrow. (b) Strength of the phase synchronization is coded by the width of the connecting lines. In (a) and (b) solid lines correspond to external pacing (first minute) and dashed lines belong to internal pacing (second minute).

asymmetry analysis we should keep in mind that, according to the instruction, the goal of the neuronal control is to keep the peripheral, muscular oscillation as regular as possible. This control is based on the proprioceptive feedback, i.e., the brain areas responsible for generating and/or controlling the muscular oscillation permanently receive information on the muscular action. Apart from monitoring the peripheral oscillation, these brain areas have to react appropriately to the deviations of the actual peripheral motion from a periodic one. For this, the brain areas have to be sensitive to the phase dynamics of the muscular oscillation. We observe the following patterns of interaction:

External pacing (first minute): PMC and LC are stronger influenced by SMC than vice versa. This may be a correlate of PMC and LC being strongly sensitive to the activity of SMC, in order to maintain a periodic action of SMC. Put otherwise, PMC and LC stabilize SMC by adapting to its oscillation. Furthermore, LC adapts to PMC. The strongest adaptation is, thus, found in LC, an area which is important for time estimation. SAC interacts symmetrically with all other brain areas under consideration.

Internal pacing (second minute): The picture is different compared to the first minute. SMC and LC as well as SMC and PMC are now interacting in a symmetric way. LC adapts to the phase dynamics of PMC. In this way LC may stabilize the periodic action of PMC. SAC plays a completely different role compared to the external pacing: Instead of interacting symmetrically, it adapts its phase dynamics to all other brain areas under consideration. In this way SAC, supported by LC, plays the role of an inner clock necessary for internal rhythm generation. This fits nicely to previous behavioral results which point out the importance of an inner voice for the internal generation of rhythmic movements.[43)]

We also investigated the degree of asymmetry between the muscular activity (RF) and all four brain areas under consideration. During both first and second minute in all pairs we obtain the same type of adaptation: The brain activity is more sensitive to the muscular activity, which may mean that the controlling brain areas adapt to the muscular activity in a way that they stabilize the periodic tapping. Although this is consistent with the above mentioned results concerning

the brain/brain-interactions, we should mention that in case of the brain/muscle-interaction the determination of asymmetry according to (2·2) is not reliable because of the high coherence and synchronization between peripheral and brain activity (see §3.1).

§5. Discussion and conclusions

With this study, we addressed the problem of experimental detection of the asymmetry of interaction of neuronal oscillators within the framework of weakly coupled oscillators theory. The technique briefly described in §2 has been tested on biophysically motivated neural oscillators, i.e. coupled Hindmarsh-Rose neurons. The results show that the pairwise analysis of phase variables of oscillators in small networks can reveal bi- or unidirectional interaction and quantify the degree of coupling asymmetry.

Single cell level oscillations often provide an inaccurate description of global oscillatory behavior of neuronal populations. Thus, we employed a macroscopic level of description by considering the dynamics of large neuronal ensembles. A new model of two ensembles of globally coupled neuronal oscillators, interacting via their mean fields, has enabled us to simulate directional interactions between sources of rhythmical activity which underlie observed signals, such as the MEG or EEG. The results of asymmetry analysis for this model demonstrate that asymmetry in interaction can be estimated for such complex systems as well.

Concerning the application of our asymmetry analysis we should mention that we operate close to the method's limits of resolution because of the small number of periods in the MEG recordings. Nevertheless, it is quite remarkable how strongly the pattern of interactions differ between external and internal pacing, although the synchronization hardly changes in the studied sources and frequency band (Fig. 8). The neurophysiological result which is suggested by our analysis, i.e., the dominant role of the secondary auditory cortex for the generation of internal rhythms, is consistent with previous behavioral studies which demonstrated the significance of an inner voice for internal rhythm generation.[43] Motivated by these results, we are going to substantiate our findings by investigating more subjects and additionally modifying the experimental protocol.

Acknowledgements

This study was supported by the IKYDA-DAAD bilateral program, the Volkswagen Foundation (76761), the German Israeli Foundation (I-667-81.1/2000), and the ZAM, Res. Ctr. Jülich (JIME03).

References

1) H. D. I. Abarbanel, *Analysis of Observed Chaotic Data* (Springer-Verlag, New York, 1996).
2) H. Kantz and T. Schreiber, *Nonlinear Time Series Analysis* (Cambridge University Press, Cambridge, 1997).
3) M. G. Rosenblum, A. S. Pikovsky, J. Kurths, C. Schäfer and P. A. Tass, *Handbook of Biological Physics* **4** (Elsevier, Amsterdam, 2001), p. 279.

4) S. J. Schiff, P. So, T. Chang, R. E. Burke and T. Sauer, Phys. Rev. E **54** (1996), 6708.
5) P. Tass, M. G. Rosenblum, J. Weule, J. Kurths, A. S. Pikovsky, J. Volkmann, A. Schnitzler and H. -J. Freund, Phys. Rev. Lett. **81** (1998), 3291.
6) M. Le van Quyen, C. Adam, M. Baulac, J. Martinerie and F. J. Varela, Brain Research **792** (1998), 24.
7) J. Arnhold, P. Grassberger, K. Lehnertz and C. E. Elger, Physica D **134** (1999), 419.
8) E. Rodriguez, N. George, J. -P. Lachaux, J. Martinerie, B. Renault and F. J. Varela, Nature **397** (1999), 430.
9) A. Neiman, X. Pei, D. F. Russell, W. Wojtenek, L. Wilkens, F. Moss, H. A. Braun, M. T. Huber and K. Voigt, Phys. Rev. Lett. **82** (1999), 660.
10) A. B. Neiman and D. F. Russell, Phys. Rev. Lett. **88** (2002), 138103.
11) R. D. Traub, R. Miles and R. K. S. Wong, Science **243** (1989), 1319.
12) P. F. Pinsky and J. Rinzel, J. Comput. Neurosci. **1** (1994), 39.
13) P. A. Tass, T. Fieseler, J. Dammers, K. Dolan, P. Morosan, M. Majtanik, F. Boers, A. Muren, K. Zilles and G. R. Fink, Phys. Rev. Lett. **90** (2003), 088101.
14) P. A. Tass, *Phase Resetting in Medicine and Biology — Stochastic Modelling and Data Analysis* (Springer, Berlin, 1999).
15) P. A. Tass, Biol. Cybern. **87** (2002), 102.
16) P. A. Tass, Phys. Rev. E **66** (2002), 036226.
17) F. Mormann, K. Lehnertz, P. David and C. E. Elger, Physica D **144** (2000), 358.
18) R. Quian Quiroga, J. Arnhold and P. Grassberger, Phys. Rev. E **61** (2000), 5142.
19) C. Schäfer, M. G. Rosenblum, J. Kurths and H.-H. Abel, Nature **392** (1998), 239.
20) A. Pikovsky, M. Rosenblum and J. Kurths, *Synchronization. A Universal Concept in Nonlinear Sciences* (Cambridge University Press, Cambridge, 2001).
21) J. Bhattacharya, H. Petsche, U. Feldmann and B. Rescher, Neurosc. Lett. **311** (2001), 29.
22) M. G. Rosenblum and A. S. Pikovsky, Phys. Rev. E **64** (2001), 045202.
23) M. G. Rosenblum, L. Cimponeriu, A. Bezerianos, A. Patzak and R. Mrowka, Phys. Rev. E **65** (2002), 041909.
24) A. M. Wing and A. B. Kristofferson, Percept. Psychophys. **14** (1973), 5.
25) S. M. Rao, D. L. Harrington, K. Y. Haaland, J. A. Bobholz, R. W. Cox and J. R. Binder, J. Neurosci. **17** (1997), 5528.
26) A. A. Ioannides, J. P. R. Bolton and C. J. S. Clarke, Inverse Problems **6** (1990), 523.
27) C. W. J. Granger, Econometrica **37** (1969), 424.
28) T. Schreiber, Phys. Rev. Lett. **85** (2000), 461.
29) M. Paluš, V. Komárek, Z. Hrnčiř and K. Štěrbová, Phys. Rev. E **63** (2001), 046211.
30) Y. Kuramoto, *Chemical Oscillations, Waves and Turbulence* (Springer, Berlin, 1984).
31) M. G. Rosenblum, A. S. Pikovsky and J. Kurths, Phys. Rev. Lett. **76** (1996), 1804.
32) A. S. Pikovsky, Sov. J. Commun. Technol. Electron. **31** (1986), 81.
33) B. P. Bezruchko, V. Ponomarenko, A. S. Pikovsky and M. G. Rosenblum, Chaos **13** (2003).
34) R. Quian Quiroga, A. Kraskov, T. Kreuz and P. Grassberger, Phys. Rev. E **65** (2002), 041903.
35) J. L. Hindmarsh and R. M. Rose, Proc. R. Soc. London B **221** (1984), 87.
36) Y. Kuramoto, *Lecture Notes in Phys.* **39** (Springer, New York, 1975).
37) P. C. Bressloff, Phys. Rev. E **60** (1999), 2160.
38) K. Okuda and Y. Kuramoto, Prog. Theor. Phys. **91** (1991), 1159.
39) K. Okuda, Physica D **63** (1993), 424.
40) S. K. Han, C. Kurrer and Y. Kuramoto, Phys. Rev. Lett. **75** (1995), 3190.
41) N. Nakagawa and Y. Kuramoto, Prog. Theor. Phys. **89** (1993), 313.
42) N. Nakagawa and Y. Kuramoto, Physica D **75** (1994), 74.
43) J. Pich, Span. J. Psychol. **3** (2000), 63 .